J Neurosurg 119:845–852, 2013

Phase II clinical study on intraoperative photodynamic therapy with talaporfin sodium and semiconductor laser in patients with malignant brain tumors

Clinical article

Yoshihiro Muragaki, M.D., Ph.D.,[1,2] Jiro Akimoto, M.D., D.Med.Sci.,[3] Takashi Maruyama, M.D., Ph.D.,[1,2] Hiroshi Iseki, M.D., Ph.D.,[1,2] Soko Ikuta, Ph.D.,[1] Masayuki Nitta, M.D., Ph.D.,[1,2] Katsuya Maebayashi, M.D., Ph.D.,[4] Taiichi Saito, M.D., Ph.D.,[1,5] Yoshikazu Okada, M.D., Ph.D.,[2] Sadao Kaneko, M.D.,[6] Akira Matsumura, M.D., Ph.D.,[7] Toshihiko Kuroiwa, M.D., Ph.D.,[8] Katsuyuki Karasawa, M.D., Ph.D.,[9] Yoichi Nakazato, M.D., Ph.D.,[10] and Takamasa Kayama, M.D., Ph.D.[11]

[1]Faculty of Advanced Techno-Surgery, Institute of Advanced Biomedical Engineering and Science, and Departments of [2]Neurosurgery and [4]Radiation Oncology, Tokyo Women's Medical University, Tokyo; [3]Department of Neurosurgery, Tokyo Medical University, Tokyo; [5]Department of Neurosurgery, Hiroshima University, Hiroshima; [6]Kashiwaba Neurosurgical Hospital, Sapporo; [7]Department of Neurosurgery, University of Tsukuba, Ibaragi; [8]Department of Neurosurgery, Osaka Medical College, Osaka; [9]Department of Radiology, Tokyo Metropolitan Cancer and Infectious Diseases Center, Komagome Hospital, Tokyo; [10]Department of Human Pathology, Gunma University Graduate School of Medicine, Gunma; and [11]Department of Neurosurgery, Yamagata University, Yamagata, Japan

Object. The objective of the present study was to perform a prospective evaluation of the potential efficacy and safety of intraoperative photodynamic therapy (PDT) using talaporfin sodium and irradiation using a 664-nm semiconductor laser in patients with primary malignant parenchymal brain tumors.

Methods. In 27 patients with suspected newly diagnosed or recurrent primary malignant parenchymal brain tumors, a single intravenous injection of talaporfin sodium (40 mg/m^2) was administered 1 day before resection of the neoplasm. The next day after completion of the tumor removal, the residual lesion and/or resection cavity were irradiated using a 664-nm semiconductor laser with a radiation power density of 150 mW/cm^2 and a radiation energy density of 27 J/cm^2. The procedure was performed 22–27 hours after drug administration. The study cohort included 22 patients with a histopathologically confirmed diagnosis of primary malignant parenchymal brain tumor. Thirteen of these neoplasms (59.1%) were newly diagnosed glioblastomas multiforme (GBM).

Results. Among all 22 patients included in the study cohort, the 12-month overall survival (OS), 6-month progression-free survival (PFS), and 6-month local PFS rates after surgery and PDT were 95.5%, 91%, and 91%, respectively. Among patients with newly diagnosed GBMs, all these parameters were 100%. Side effects on the skin, which could be attributable to the administration of talaporfin sodium, were noted in 7.4% of patients and included rash (2 cases), blister (1 case), and erythema (1 case). Skin photosensitivity test results were relatively mild and fully disappeared within 15 days after administration of photosensitizer in all patients.

Conclusions. Intraoperative PDT using talaporfin sodium and a semiconductor laser may be considered as a potentially effective and sufficiently safe option for adjuvant management of primary malignant parenchymal brain tumors. The inclusion of intraoperative PDT in a combined treatment strategy may have a positive impact on OS and local tumor control, particularly in patients with newly diagnosed GBMs. Clinical trial registration no.: JMA-IIA00026 (https://dbcentre3.jmacct.med.or.jp/jmactr/App/JMACTRS06/JMACTRS06.aspx?seqno=862).
(http://thejns.org/doi/abs/10.3171/2013.7.JNS13415)

Key Words • **malignant brain tumor** • **malignant glioma** • **oncology** • **photodynamic therapy** • **talaporfin sodium** • **outcome**

Malignant brain tumors are characterized by invasive growth into adjacent normal neuronal tissue. Therefore, it is crucial that their man-

This article contains some figures that are displayed in color online but in black-and-white in the print edition.

Abbreviations used in this paper: GBM = glioblastoma multiforme; OS = overall survival; PDT = photodynamic therapy; PFS = progression-free survival; PS = performance status; 5-ALA = 5-aminolevulinic acid.

agement is directed not only to maximal possible resection (while ensuring preservation of the functionally important anatomical structures), but on suppressing the growth of the residual infiltrative tumor cells. Despite aggressive surgical removal followed by postoperative radiotherapy and chemotherapy, between 50% and 85% of WHO Grade IV gliomas recur locally.[9,16] This emphasizes the need for additional options to improve their growth control.

Photodynamic therapy (PDT) is a treatment method that involves administration of a photosensitizer that accumulates in tumor tissue and newly formed neoplastic vessels. During subsequent irradiation with a laser beam of a specific wavelength, the photosensitizer undergoes a photochemical reaction that produces singlet oxygen possessing strong oxidation properties that cause alteration of the cells. Because singlet oxygen has a short lifetime (0.04–4 μsec), the PDT-induced cell death is realized only locally in the areas irradiated by the laser beam.[2,7,8,15]

Talaporfin sodium (mono-L-aspartyl chlorine e6, or NPe6) is a relatively novel photosensitizer for PDT. Its administration in combination with a semiconductor laser has been approved in Japan for clinical use in cases of early stage lung cancer. Nonclinical pharmacological studies directed to its possible application for management of malignant brain tumors were initiated starting in 2001.[12–14] Experiments with glioblastoma cell lines demonstrated that such therapy induces mitochondrial apoptotic cell loss accompanied by tumor necrosis.[13,14] Our recent single-center pilot clinical study on the use of talaporfin sodium and a semiconductor laser in patients with malignant gliomas demonstrated promising results with regard to tumor response rates and treatment safety.[1] Therefore, the present open-label, prospective, multicenter clinical trial was initiated for evaluation of the potential efficacy and safety of such therapy. This study was the first investigator-initiated clinical trial in Japan that planned to assess the use of talaporfin sodium and a semiconductor laser for intraoperative PDT as part of a combined management of primary malignant parenchymal brain tumors.

Methods

Patients with suspected primary malignant parenchymal brain tumors, either newly diagnosed or recurrent, which according to preoperative neuroimaging corresponded to a WHO histopathological grade of III or IV,[11] were enrolled in this study. The recruitment of patients and analysis of treatment efficacy were mainly focused on newly diagnosed glioblastoma multiforme (GBM). The main inclusion criteria included agreement of the patient to provide written informed consent to participate in the study; age between 20 and 69 years at the time of informed consent; performance status (PS) score of 0, 1, 2, or 3 according to Eastern Cooperative Oncology Group PS scale (a PS score of 3 was accepted only when the score was attributable to neurological symptoms caused by the tumor); supratentorial location of the tumor not including neoplasms originating from the optic pathways and pituitary gland; absence of subarachnoid dissemination; and eligibility for aggressive resection of the lesion. The main exclusion criterion was a history of photosensitivity or porphyria.

Study Design

This prospective clinical trial was developed and carried out in 2 neurosurgical centers with well-established neurooncology programs, namely Tokyo Women's Medical University and Tokyo Medical University. An open-label, investigator-initiated clinical study was conducted in accordance with the Declaration of Helsinki. The research protocol was approved by the Pharmaceuticals and Medical Devices Agency of Japan as well as by the ethics committees and institutional review boards of both participating universities. A special review board was formed for central radiology assessment, evaluation of data related to treatment efficacy and safety, and handling of the enrolled cases and overall data management. Additionally, a pathology board was created for central review of the permanent formalin-fixed tissue specimens to determine the histopathological tumor type and grade. The 3-year study period was scheduled from March 21, 2009, to February 28, 2012. The clinical trial information for this study can be found at https://dbcentre3.jmacct.med.or.jp/jmactr/App/JMACTRS06/JMACTRS06.aspx?seqno=862.

Patients who were considered eligible for enrollment into study received a single intravenous injection of talaporfin sodium (Laserphyrin, Meiji Seika Pharma Co., Ltd.) in a dose of 40 mg/m^2 on an inpatient basis 1 day prior to undergoing the elective craniotomy. The next day, surgery was done, the neoplasm was resected, and irradiation of the resection cavity with a 664-nm semiconductor laser beam (Panasonic Healthcare Co., Ltd.), with a diameter of 1.5 cm, radiation power density of 150 mW/cm^2, and radiation energy density of 27 J/cm^2, was performed. Particular emphasis was put on irradiation of the areas at risk for recurrence, such as the genu of the corpus callosum.[9] If tumor resection was incomplete and the residual lesion was macroscopically identified, additional irradiation by the laser was applied at 1 to 3 sites with avoidance of overlap of the irradiation areas. In all cases laser irradiation was done 22–27 hours after administration of talaporfin sodium.

Postoperative Treatment and Follow-Up

Postoperatively all patients with newly diagnosed gliomas underwent fractionated radiotherapy (total dose 60 Gy) with concomitant and adjuvant chemotherapy using ACNU (in cases of WHO Grade III tumors) or temozolomide[18] (in cases of GBM). Patients with recurrent neoplasms were treated according to the preference of their doctors, taking into consideration the details of the primary management.

Adverse effects of treatment were graded according to the Common Terminology Criteria for Adverse Events version 3.0.[3] Follow-up examinations were performed every 2–3 months and included physical and neurological assessments with evaluation of PS score, blood and urine tests, and contrast-enhanced MRI. Tumor progression was defined as a 25% or greater increase in the volume of the contrast-enhanced lesion or the appearance of

new brain lesions. At the time of recurrence the salvage treatment was applied according to the preference of the individual doctors and usually included a combination of re-resection, second-line chemotherapy, and/or vaccine therapy.

End Point Evaluation

The primary end point of the study was overall survival (OS) rate at 12 months after PDT. Secondary end points were progression-free survival (PFS) and local PFS rates at 6 months after PDT. The OS, PFS, and local PFS were all estimated from the date of surgery. Additionally, in cases with a maximal diameter of the residual neoplasm of 16 mm or more, the overall tumor response to treatment was evaluated. All brain MRI data before surgery and during follow-up were assessed by review board members. Safety end points included rates of adverse events, side effects, and results of skin photosensitivity testing.

Data Analysis

Analysis of the treatment efficacy was done in all patients who underwent PDT based on administration of talaporfin sodium and intraoperative laser irradiation of the residual neoplasm and/or resection cavity if the diagnosis of primary malignant parenchymal brain tumor was confirmed by the pathology review board after investigation of the permanent formalin-fixed tissue sections (study cohort). Separate analysis of the treatment efficacy was also done in the subgroup of patients with newly diagnosed GBMs. Survival was assessed using the Kaplan-Meier method. Analysis of the treatment safety was done in all patients initially enrolled into the study who received talaporfin sodium.

Results

Patient Characteristics

Detailed characteristics of patients enrolled in the study are presented in Table 1. In all, 27 patients initially received talaporfin sodium. However, 3 patients were deemed ineligible for study participation during surgery and did not receive irradiation with the laser based on the results of the intraoperative histopathological investigation of the resected tissue on the frozen sections, which revealed lymphoma, low-grade glioma, and cavernoma (1 case each). Additionally, 2 patients were excluded from the study later on because the pathology review board did not confirm the diagnosis of a primary malignant parenchymal brain tumor based on the postoperative examination of the permanent formalin-fixed tissue sections. Therefore, the study cohort included 22 patients with a male/female ratio of 1:1 and a median age of 50.5 years (range 24–69 years). The frontal lobe was affected most frequently (59.1% of cases). In 72.7% of patients the tumor was located within or close to eloquent brain areas. Total, subtotal (> 90% of the lesion volume), and partial resections of the neoplasm were performed in 36.4%, 50%, and 13.6% of cases, respectively. No significant differences in clinical characteristics were observed between the entire group of initially enrolled patients (n = 27) and the study cohort (n = 22). Thirteen (59.1%) of 22 patients included in the study cohort had newly diagnosed GBMs and corresponded to recursive partitioning analysis Classes III (4 cases), IV (5 cases), and V (4 cases).[6]

Treatment Efficacy

Among all 22 patients included in the study cohort, 1 death occurred within 12 months after surgery. This patient died 3.4 months after resection and PDT of a newly diagnosed gliosarcoma due to local progression of the tumor. Therefore, the 12-month OS rate was 95.5%. Two tumors demonstrated progression despite treatment within 6 months after surgery, and both recurrences were local. Therefore, the 6-month PFS and local PFS rates were 91%. The maximum length of follow-up was 38.6 months. The median OS was 27.9 months (95% CI lower, 24.8 months; upper, not estimated), the median PFS was 20 months (95% CI lower, 10.3 months; upper, not estimated), and the median local PFS was 22.5 months (95% CI lower, 17.2 months; upper, not estimated).

Among 13 patients with newly diagnosed GBM, the 12-month OS, 6-month PFS, and 6-month local PFS rates after surgical removal of the tumor and PDT were all 100% (Fig. 1). In this subgroup the maximum length of follow-up was 32.0 months. The median OS was 24.8 months (95% CI 18.5–32.0 months), the median PFS was 12.0 months (95% CI 10.3–24.2 months), and the median local PFS was 20.0 months (95% CI 16.2–32.0 months).

In only 1 patient was it possible to evaluate the overall tumor response to treatment. In this case, a newly diagnosed GBM showed complete response 4 months after surgery and PDT.

Treatment Safety

Among all 27 patients who received talaporfin sodium the day before surgery, serious adverse events were noted postoperatively in 6 patients (22.2%). These included aphasia (2 cases) and hemiplegia, hemiparesis, unilateral blindness, visual field defect, homonymous hemianopia, postoperative pyrexia, and infection (1 case each). The overall frequency and distribution of postoperative adverse events were within the range of our usual neurosurgical practice in cases of primary malignant parenchymal brain tumors, and their causal relationships with administration of talaporfin sodium and/or intraoperative laser irradiation were very unlikely. None of these adverse events resulted in the death of a patient.

The laboratory test results in all patients were abnormal, most frequently with an increase in γ-glutamyltransferase (59.3%), alanine aminotransferase (48.1%), aspartate aminotransferase (37.0%), blood alkaline phosphatase (25.9%), and blood lactate dehydrogenase (22.2%). In 18 (66.7%) of 27 patients such abnormalities could be considered as side effects after administration of talaporfin sodium. Postoperative adverse events by system organs, particularly abnormal liver function, were relatively frequent but never exceeded Grade 3 toxicity (Table 2). Only 2 patients (7.4%) had skin disorders, which could be con-

TABLE 1: Characteristics of patients enrolled into study

Demographics & Clinical Characteristics	Value*		
	Initially Enrolled Patients (n = 27)	Study Cohort	
		Total (n = 22)	Newly Diagnosed GBM (n = 13)
age in yrs			
mean ± SD	47.1 ± 13.5	48.1 ± 13.5	46.0 ± 14.1
median (range)	50.0 (24–69)	50.5 (24–69)	49.0 (24–69)
sex			
male	13 (48.1)	11 (50.0)	6 (46.2)
female	14 (51.9)	11 (50.0)	7 (53.8)
histopathological type of tumor†			
GBM	13 (48.1)	13 (59.1)	13 (100.0)
gliosarcoma	1 (3.7)	1 (4.5)	0 (0)
anaplastic astrocytoma	3 (11.1)	3 (13.6)	0 (0)
anaplastic oligoastrocytoma	2 (7.4)	2 (9.1)	0 (0)
anaplastic oligodendroglioma	2 (7.4)	2 (9.1)	0 (0)
pilocytic astrocytoma w/ anaplastic features	1 (3.7)	1 (4.5)	0 (0)
oligodendroglioma	2 (7.4)	0 (0)	0 (0)
central review not performed‡	3 (11.1)	0 (0)	0 (0)
WHO grade†			
IV	14 (51.9)	14 (63.6)	13 (100.0)
III	8 (29.6)	8 (36.4)	0 (0)
II	2 (7.4)	0 (0)	0 (0)
central review not performed‡	3 (11.1)	0 (0)	0 (0)
tumor status			
newly diagnosed	26 (96.3)	21 (95.5)	13 (100.0)
recurrent	1 (3.7)	1 (4.5)	0 (0)
tumor location			
frontal lobe	16 (59.3)	13 (59.1)	7 (53.8)
temporal lobe	5 (18.5)	3 (13.6)	2 (15.4)
parietal lobe	4 (14.8)	4 (18.2)	3 (23.1)
occipital lobe	2 (7.4)	2 (9.1)	1 (7.7)
tumor side			
rt	13 (48.1)	12 (54.5)	8 (61.5)
lt	14 (51.9)	10 (45.5)	5 (38.5)
tumor functional grade			
located in eloquent area	13 (48.1)	12 (54.5)	7 (53.8)
adjacent to eloquent area	6 (22.2)	4 (18.2)	2 (15.4)
located in noneloquent area	8 (29.6)	6 (27.3)	4 (30.8)
PS before treatment§			
0	14 (51.9)	10 (45.5)	3 (23.1)
1	10 (37.0)	9 (40.9)	8 (61.5)
2	0 (0)	0 (0)	0 (0)
3	3 (11.1)	3 (13.6)	2 (15.4)
extent of tumor resection			
total	9 (33.3)	8 (36.4)	5 (38.5)
subtotal (>90% of lesion vol)	13 (48.1)	11 (50.0)	8 (61.5)
partial	5 (18.5)	3 (13.6)	0 (0)

* Unless otherwise stated, values represent cases (%).
† According to central review based on WHO criteria.
‡ These patients did not receive laser irradiation during surgery due to results of the intraoperative histopathological investigation of the resected tissue on the frozen sections and exclusion of the diagnosis of primary malignant parenchymal brain tumor.
§ According to the Eastern Cooperative Oncology Group Performance Status Scale.

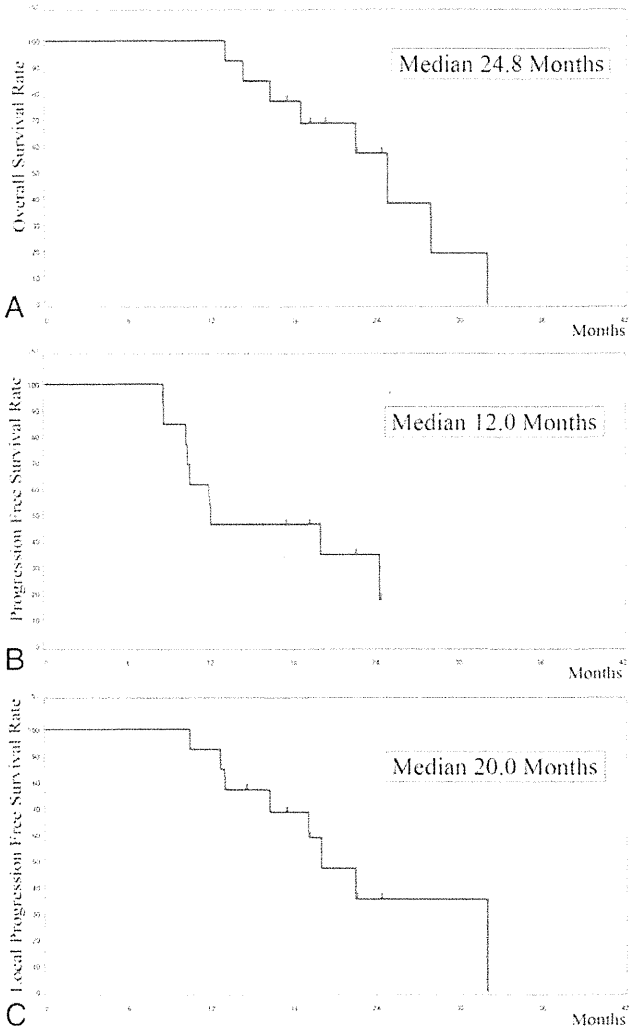

Fig. 1. Kaplan-Meier curves for OS **(A)**, PFS **(B)**, and local PFS **(C)** in the subgroup of patients with newly diagnosed GBM included in the study cohort. Censored observations are marked.

sidered as side effects after administration of talaporfin sodium. It included rash (2 cases), blister (1 case), and erythema (1 case).

Photosensitivity test results were relatively mild and most patients had a score of 1 (barely perceptible erythema) or 2 (distinct erythema); no patient had a score of 3 (marked erythema or edema). These reactions completely disappeared within 4, 8, and 15 days after administration of talaporfin sodium in 55.6%, 77.8%, and 100% of patients, respectively (Table 3).

Discussion

Management of primary malignant parenchymal brain tumors represents a significant challenge. According to the latest edition of the Japan Brain Tumor Registry, 1-, 2-, and 3-year survival rates of patients with high-grade gliomas constitute 64%, 37%, and 28%, respectively.[5] The poor survival rates are mainly due to an inability to perform complete removal of the neoplasm due to its infiltrative growth into functionally important neuronal structures, as well as the limited effectiveness of the postoperative radiotherapy and chemotherapy. Therefore, finding additional effective and safe treatment options in such cases is required.

As a highly selective treatment with minimal injury to the adjacent normal structures, PDT has demonstrated promising potential for management of the various cancers and nonneoplastic disorders, such as age-related macular degeneration, local infection, dermatological diseases, arteriosclerosis, and rheumatoid arthritis.[7] However, despite a large amount of basic and clinical research conducted during several decades and directed on testing of the various photosensitizers, light sources, irradiation types, and treatment regimens, PDT still was not approved to be used as a standard treatment for malignant brain tumors.[2,10] During the last decade there was considerable interest in the use of 5-aminolevulinic acid (5-ALA) in the surgical management of gliomas. Nevertheless, while its application for photodynamic diagnosis and fluorescence-guided resection was associated with a significant impact on effectiveness of tissue sampling, tumor resection rates, and clinical outcomes,[4,17] the attempts to use this photosensitizer for PDT were not so impressive.[2] These unimpressive results might be particularly caused by insufficient incorporation of the drug in the neoplastic cells, especially in necrotic regions and at the periphery of the neoplasm.[2]

In the present study PDT was based on administration of the relatively novel second-generation photosensitizer talaporfin sodium. This water-soluble compound is derived from plant chlorophyll. In the living body it binds to albumin and does not pass the blood-brain barrier. In neoplastic cells it is primarily distributed in the lysosomes.[14] Compared with conventional photosensitizers, talaporfin sodium is activated by light with longer wavelengths; therefore, its light absorption is not affected by hemoglobin and penetrates deeper.[13] Additionally, talaporfin sodium more selectively accumulates in glioma tissue, is rapidly eliminated from the normal tissues, and is less likely to cause adverse reactions.[14] It was demonstrated that PDT based on administration of talaporfin sodium with subsequent irradiation using a 664-nm laser led to necrosis and apoptosis of cultured human glioblastoma cells[13] and experimental tumors[14] in a dose- and time-dependent fashion. The adverse effects on the peritumoral brain were limited to mild temporary edema, and no damage to neurons or the myelin sheath was observed.[14] A pilot clinical study on 14 adult patients with unresectable malignant gliomas showed a median PFS of 23 months in newly diagnosed neoplasms.[1] In concordance, in our present prospective investigation, which included 21 patients with newly diagnosed high-grade gliomas treated according to strict research protocol, the median local PFS constituted 22.5 months.

The most impressive results of our study were obtained in patients with a newly diagnosed GBM. In this subgroup, the 12-month OS and 6-month PFS rates were 100%, and the median OS and median PFS were 24.8 and 12.0 months, respectively. These rates compare favorably

TABLE 2: Frequency of adverse events and side effects by grade*

System Organ Class†	No. of Patients (%)					
	Grade 1	Grade 2	Grade 3	Grade 4	Grade 5	Total (n = 27)
adverse events						
investigations	3 (11.1)	12 (44.4)	10 (37.0)	2 (7.4)	0 (0.0)	27 (100.0)
gastrointestinal disorders	5 (18.5)	16 (59.3)	0 (0.0)	0 (0.0)	0 (0.0)	21 (77.8)
general disorders & administration site conditions	15 (55.6)	6 (22.2)	0 (0.0)	0 (0.0)	0 (0.0)	21 (77.8)
nervous system disorders	1 (3.7)	17 (63.0)	2 (7.4)	0 (0.0)	0 (0.0)	20 (74.1)
skin & subcutaneous tissue disorders	10 (37.0)	8 (29.6)	0 (0.0)	0 (0.0)	0 (0.0)	18 (66.7)
injury, poisoning, & procedural complications	9 (33.3)	6 (22.2)	0 (0.0)	0 (0.0)	0 (0.0)	15 (55.6)
eye disorders	7 (25.9)	1 (3.7)	1 (3.7)	0 (0.0)	0 (0.0)	9 (33.3)
infections & infestations	1 (3.7)	3 (11.1)	2 (7.4)	0 (0.0)	0 (0.0)	6 (22.2)
renal & urinary disorders	3 (11.1)	2 (7.4)	0 (0.0)	0 (0.0)	0 (0.0)	5 (18.5)
psychiatric disorders	4 (14.8)	0 (0.0)	0 (0.0)	0 (0.0)	0 (0.0)	4 (14.8)
respiratory, thoracic, & mediastinal disorders	4 (14.8)	0 (0.0)	0 (0.0)	0 (0.0)	0 (0.0)	4 (14.8)
vascular disorders	0 (0.0)	0 (0.0)	4 (14.8)	0 (0.0)	0 (0.0)	4 (14.8)
musculoskeletal & connective tissue disorders	1 (3.7)	2 (7.4)	0 (0.0)	0 (0.0)	0 (0.0)	3 (11.1)
blood & lymphatic system disorders	1 (3.7)	1 (3.7)	0 (0.0)	0 (0.0)	0 (0.0)	2 (7.4)
metabolism & nutrition disorders	0 (0.0)	0 (0.0)	2 (7.4)	0 (0.0)	0 (0.0)	2 (7.4)
cardiac disorders	1 (3.7)	0 (0.0)	0 (0.0)	0 (0.0)	0 (0.0)	1 (3.7)
ear & labyrinth disorders	1 (3.7)	0 (0.0)	0 (0.0)	0 (0.0)	0 (0.0)	1 (3.7)
side effects						
investigations	7 (25.9)	6 (22.2)	5 (18.5)	0 (0.0)	0 (0.0)	18 (66.7)
skin & subcutaneous tissue disorders	1 (3.7)	1 (3.7)	0 (0.0)	0 (0.0)	0 (0.0)	2 (7.4)

* According to the Cancer Therapy Evaluation Program.[3]

† According to the Medical Dictionary for Regulatory Activities version 14.1 (http://www.meddra.org).

with contemporary results obtained in such tumors with standard treatment. In a global Phase III randomized controlled study on radiotherapy with concomitant and adjuvant temozolomide for GBM, Stupp et al.[18] demonstrated a 12-month OS rate of 61%, a 6-month PFS rate of 54%, a median OS of 14.6 months, and a median PFS of 6.9 months. In the series by Stummer et al.[17] on fluorescence-guided resection of malignant gliomas with the use of 5-ALA, the 6-month PFS rate was 41% and the median PFS period was 5.1 months. Moreover, in our patients with a newly diagnosed GBM, the median local PFS was nearly two times longer than the median PFS (20.0 vs 12.0 months). It can therefore be speculated that prolonged survival was caused by improved local tumor growth control due to intraoperative PDT. It should be emphasized that in the present series all patients with newly diagnosed GBM underwent either total or subtotal resection. Aggressive removal of the tumor may be an important prerequisite for clinical effectiveness of intraoperative PDT, since the penetration depth of a laser is approximately 2.5–5 mm; therefore, the corresponding effective distance for irradiation is limited to 0.75–1.5 cm.[1,2] The limitations of the efficacy of PDT in bulky target tissues and recurrent tumors have been demonstrated.[1] It is also possible that metabolically active infiltrating tumor cells in the periphery of the GBM may be more sensitive to PDT because of incorporation of a greater amount of photosensitizer. It was reported that the tissue concentration of a photosensitizer directly correlates with the grade of malignancy of the neoplasm.[2]

In the present study PDT showed a high level of safe-

TABLE 3: Skin photosensitivity test results in 27 patients*

No. of Days†	No. of Patients (%)	Cumulative No. of Patients (%)
3	4 (14.8)	4 (14.8)
4	11 (40.7)	15 (55.6)
8	6 (22.2)	21 (77.8)
10	1 (3.7)	22 (81.5)
13	2 (7.4)	24 (88.9)
14	1 (3.7)	25 (92.6)
15	2 (7.4)	27 (100)

* For the skin photosensitivity test, between 11 a.m. and 2 p.m., the back of the individual's hand was exposed to direct sunlight for 5 minutes, and the occurrence of any photosensitivity reaction, such as erythema, was assessed. In cases in which photosensitivity reactions were detected, the subject was kept shielded from light until the reaction disappeared, and the skin photosensitivity test was subsequently repeated.

† From administration of talaporfin sodium to disappearance of reaction.

ty. While laboratory investigations have frequently revealed abnormalities likely attributable to the administration of talaporfin sodium, only 2 patients (7.4%) had definite symptoms on the skin, which did not exceed Grade 2 toxicity. In no case did we encounter brain edema or cerebral infarction, which may complicate PDT.[1,2] Therefore, the risk of clinically significant side effects caused by the administration of talaporfin sodium and intraoperative irradiation of the residual tumor and peritumoral brain with a 664-nm laser 22–27 hours thereafter may be considered low. Moreover, according to photosensitivity test results, any reactions completely disappeared in all patients within 15 days after administration of the drug.

The main limitations of the present study are related to its design. A nonrandomized noncontrolled prospective investigation was performed in just 2 neurosurgical centers with well-established neurooncology programs and enrolled a limited number of highly selected cases with rather heterogeneous histopathological diagnoses of malignant parenchymal brain tumors. It is evident that to prove clinical efficacy of the intraoperative PDT with talaporfin sodium and a semiconductor laser, further carefully designed Phase III studies should be performed in a sufficiently large number of patients with possible initial stratification according to tumor resection rate. Testing of the proposed treatment method is also planned in cases of low-grade gliomas and in incompletely resected benign extraaxial neoplasms, such as pituitary adenomas and meningiomas. Since appropriate use of equipment for PDT requires specific skills, the dedicated training program for neurosurgeons is currently under organization. Finally, advanced experimental investigations directed at further understanding the basic mechanisms of the therapeutic effectiveness of intraoperative PDT are also required, and additional studies to search for the most optimal treatment regimens should be continued as well.

Conclusions

The results of the present study demonstrate that novel PDT based on administration of talaporfin sodium and subsequent irradiation with a 664-nm semiconductor laser may provide an additional benefit to the combined management of primary malignant parenchymal brain tumors through possible improvement of their local growth control, which, in turn, may lead to prolongation of the patient's survival. The therapy seems sufficiently safe with a minimal risk of serious side effects. Therefore, application of the intraoperative PDT along with aggressive resection, radiotherapy, and chemotherapy may be of clinical significance, particularly in patients with newly diagnosed GBM.

Disclosure

This study was supported by grants of an open-label study of photodynamic therapy with ME2906 and PNL6405CNS in patients with malignant brain tumors by Center for Clinical Trials, Japan Medical Association, Funding Program for World-Leading Innovative R&D on Science and Technology (FIRST Program) by the Japan Society for the Promotion of Science (JSPS), and Strategic international standardization acceleration action plan by METI (Ministry of Economy, Trade and Industry).

Author contributions to the study and manuscript preparation include the following. Conception and design: Muragaki, Akimoto, Iseki, Maebayashi, Matsumura, Kuroiwa, Nakazato, Kayama. Acquisition of data: Muragaki, Akimoto, Ikuta, Nitta, Saito, Kaneko. Analysis and interpretation of data: Muragaki, Akimoto, Ikuta, Karasawa. Drafting the article: Muragaki. Critically revising the article: all authors. Reviewed submitted version of manuscript: all authors. Approved the final version of the manuscript on behalf of all authors: Muragaki. Statistical analysis: Muragaki, Ikuta. Administrative/technical/material support: Maruyama, Iseki, Nitta, Maebayashi, Saito, Okada, Kaneko, Matsumura, Kuroiwa, Karasawa, Nakazato, Kayama. Study supervision: Muragaki, Iseki, Maebayashi, Okada, Matsumura, Kuroiwa, Nakazato, Kayama.

Acknowledgments

The authors thank all of the patients who participated in this study and the investigators from both study sites. Special thanks are devoted to Drs. Masahiko Tanaka, Norio Mitsuhashi, and Mikhail Chernov, and Mr. Takashi Sakayori (Tokyo Women's Medical University) for valuable help with clinical work and data analysis.

References

1. Akimoto J, Haraoka J, Aizawa K: Preliminary clinical report on safety and efficacy of photodynamic therapy using talaporfin sodium for malignant gliomas. **Photodiagn Photodyn Ther 9:**91–99, 2012
2. Bechet D, Mordon SR, Guillemin F, Barberi-Heyob MA: Photodynamic therapy of malignant brain tumours: a complementary approach to conventional therapies. **Cancer Treat Rev** [epub ahead of print], 2012
3. Cancer Therapy Evaluation Program: Common Terminology Criteria for Adverse Events v3.0 (CTCAE). **ctep.cancer.gov.** (http://ctep.cancer.gov/protocolDevelopment/electronic_applications/docs/ctcaev3.pdf) [Accessed July 22, 2013]
4. Colditz MJ, Jeffree RL: Aminolevulinic acid (ALA)-protoporphyrin IX fluorescence guided tumour resection. Part 1: Clinical, radiological and pathological studies. **J Clin Neurosci 19:**1471–1474, 2012
5. Committee of Brain Tumor Registry of Japan: Report of brain tumor registry of Japan (1984–2000), 12 edition. **Neurol Med Chir (Tokyo) 49 (Suppl):**1–101, 2009
6. Curran WJ Jr, Scott CB, Horton J, Nelson JS, Weinstein AS, Fischbach AJ, et al: Recursive partitioning analysis of prognostic factors in three Radiation Therapy Oncology Group malignant glioma trials. **J Natl Cancer Inst 85:**704–710, 1993
7. Dougherty TJ, Gomer CJ, Henderson BW, Jori G, Kessel D, Korbelik M, et al: Photodynamic therapy. **J Natl Cancer Inst 90:**889–905, 1998
8. Juzeniene A, Peng Q, Moan J: Milestones in the development of photodynamic therapy and fluorescence diagnosis. **Photochem Photobiol Sci 6:**1234–1245, 2007
9. Konishi Y, Muragaki Y, Iseki H, Mitsuhashi N, Okada Y: Patterns of intracranial glioblastoma recurrence after aggressive surgical resection and adjuvant management: retrospective analysis of 43 cases. **Neurol Med Chir (Tokyo) 52:**577–586, 2012
10. Kostron H: Photodynamic diagnosis and therapy and the brain. **Methods Mol Biol 635:**261–280, 2010
11. Louis DN, Ohgaki H, Wiestler OD, Cavenee WK (eds): **WHO Classification of Tumours of the Central Nervous System, ed 4.** Lyon: IARC Press, 2007
12. Matsumura H, Akimoto J, Haraoka J, Aizawa K: Uptake and retention of the photosensitizer mono-L-asparthyl chlorine e6 in experimental malignant glioma. **Lasers Med Sci 23:**237–245, 2008

13. Miki Y, Akimoto J, Yokoyama S, Homma T, Tsutsumi M, Haraoka J, et al: Photodynamic therapy in combination with talaporfin sodium induces mitochondrial apoptotic cell death accompanied with necrosis in glioma cells. **Biol Pharm Bull 36:**215–221, 2013
14. Namatame H, Akimoto J, Matsumura H, Haraoka J, Aizawa K: Photodynamic therapy of C6-implanted glioma cells in the rat brain employing second-generation photosensitizer talaporfin sodium. **Photodiagn Photodyn Ther 5:**198–209, 2008
15. Palumbo G: Photodynamic therapy and cancer: a brief sightseeing tour. **Expert Opin Drug Deliv 4:**131–148, 2007
16. Petrecca K, Guiot MC, Panet-Raymond V, Souhami L: Failure pattern following complete resection plus radiotherapy and temozolomide is at the resection margin in patients with glioblastoma. **J Neurooncol 111:**19–23, 2013
17. Stummer W, Pichlmeier U, Meinel T, Wiestler OD, Zanella F, Reulen HJ: Fluorescence-guided surgery with 5-aminolevulinic acid for resection of malignant glioma: a randomised controlled multicentre phase III trial. **Lancet Oncol 7:**392–401, 2006
18. Stupp R, Mason WP, van den Bent MJ, Weller M, Fisher B, Taphoorn MJ, et al: Radiotherapy plus concomitant and adjuvant temozolomide for glioblastoma. **N Engl J Med 352:**987–996, 2005

Manuscript submitted February 28, 2013.
Accepted July 16, 2013.
Please include this information when citing this paper: published online August 16, 2013; DOI: 10.3171/2013.7.JNS13415.
Address correspondence to: Yoshihiro Muragaki, M.D., Ph.D., Faculty of Advanced Techno-Surgery, Institute of Advanced Biomedical Engineering and Science, Tokyo Women's Medical University, 8-1 Kawada-cho, Shinjuku-ku, Tokyo 162-8666, Japan. email: ymuragaki@abmes.twmu.ac.jp.

INTERNATIONAL JOURNAL OF UROLOGY
International Journal of Urology (2013) 20, 993–999 doi: 10.1111/iju.12091

Original Article: Clinical Investigation

Ability of preoperative 3.0-Tesla magnetic resonance imaging to predict the absence of side-specific extracapsular extension of prostate cancer

Tomohiko Hara,[1] Hiroyuki Nakanishi,[1] Tohru Nakagawa,[1] Motokiyo Komiyama,[1] Takashi Kawahara,[1] Tomoko Manabe,[2] Mototaka Miyake,[2] Eri Arai,[3] Yae Kanai[3] and Hiroyuki Fujimoto[1]

[1]Urology Division, National Cancer Center Hospital, [2]Diagnostic Radiology Division, National Cancer Center Hospital, and [3]Division of Molecular Pathology, National Cancer Center Research Institute, Tokyo, Japan

Abbreviations & Acronyms
3.0-T = 3.0-Tesla
ADC = apparent diffusion coefficient
CI = confidence interval
DRE = digital rectal examination
DWI = diffusion-weighted imaging
ECE = extracapsular extension
MRI = magnetic resonance imaging
NPV = negative predictive value
OR = odds ratio
PPV = positive predictive value
PSA = prostate-specific antigen
PZ = peripheral zone
RP = radical prostatectomy
T = Tesla
T2WI = T2-weighted imaging
TRUS = transrectal ultrasonography
TZ = transitional zone

Correspondence: Tomohiko Hara M.D., Ph.D., Urology Division, National Cancer Center Hospital, Tsukiji 5-1-1, Chuo-ku, Tokyo 104-0045, Japan. Email: tomohara-jua@umin.ac.jp

Received 15 August 2012; accepted 26 December 2012. Online publication 29 January 2013

Objective: Recent studies have shown an improvement in prostate cancer diagnosis with the use of 3.0-Tesla magnetic resonance imaging. We retrospectively assessed the ability of this imaging technique to predict side-specific extracapsular extension of prostate cancer.

Methods: From October 2007 to August 2011, prostatectomy was carried out in 396 patients after preoperative 3.0-Tesla magnetic resonance imaging. Among these, 132 (primary sample) and 134 patients (validation sample) underwent 12-core prostate biopsy at the National Cancer Center Hospital of Tokyo, Japan, and at other institutions, respectively. In the primary dataset, univariate and multivariate analyses were carried out to predict side-specific extracapsular extension using variables determined preoperatively, including 3.0-Tesla magnetic resonance imaging findings (T2-weighted and diffusion-weighted imaging). A prediction model was then constructed and applied to the validation study sample.

Results: Multivariate analysis identified four significant independent predictors ($P < 0.05$), including a biopsy Gleason score of ≥8, positive 3.0-Tesla diffusion-weighted magnetic resonance imaging findings, ≥2 positive biopsy cores on each side and a maximum percentage of positive cores ≥31% on each side. The negative predictive value was 93.9% in the combination model with these four predictors, meanwhile the positive predictive value was 33.8%. Good reproducibility of these four significant predictors and the combination model was observed in the validation study sample.

Conclusions: The side-specific extracapsular extension prediction by the biopsy Gleason score and factors associated with tumor location, including a positive 3.0-Tesla diffusion-weighted magnetic resonance imaging finding, have a high negative predictive value, but a low positive predictive value.

Key words: 3.0-Tesla diffusion-weighted magnetic resonance imaging, capsular invasion, extracapsular extension, nerve-sparing radical prostatectomy, prostate cancer.

Introduction

MRI has considerable potential to improve the accuracy of prostate cancer diagnosis.[1] DWI in MRI is a non-invasive technique that provides information about cell density and diffusion restriction in cancerous tissue.[2] Recent studies have shown improved diagnostic accuracy with the combined use of 3.0-T DWI MRI and T2WI MRI for patients with prostate cancer.[3,4]

ECE of prostate cancer is an important predictor of the outcome of RP.[5,6] Many urologists have attempted to predict ECE location using various preoperative parameters, such as clinical stage, Gleason score and preoperative serum PSA level.[5,7,8] However, the preoperative diagnostic accuracy using these conventional parameters is limited. Therefore, we hypothesized that 3.0-T MRI information combined with conventional preoperative features might facilitate more accurate prediction of side-specific ECE.

Methods

Patient population

From October 2007 to August 2011, open retropubic radical prostatectomy after preoperative 3.0-T MRI examination was carried out in 396 patients at the National Cancer Center Hospital of Tokyo, Japan. Of these, 130 were excluded because they received neoadjuvant therapy, provided insufficient data for analysis or were diagnosed with tumors other than adenocarcinoma. Of the remaining patients, 132 patients who were diagnosed with T1c–T3a prostate cancer after undergoing 12-core prostate biopsy at our institution were enrolled as a primary study sample. Systematic 12-core biopsy specimens were obtained under the guidance of TRUS using an end-fire probe (B-K Medical, Herlev, Denmark). Meanwhile, a validation study sample including 134 patients who had undergone ≥10 core biopsies at other institutions was enrolled. Results of all biopsies were reviewed by two pathologists (EA and YK).

Pathological evaluation

All biopsy samples and resected specimens were evaluated by two pathologists (EA and YK). The Gleason score was obtained by summing the primary and secondary tumor grades. In our institution, the location and Gleason scores for 12 biopsy cores are recorded as a systematic part of the biopsy process. For both sides in all patients, the number and maximum percentage of positive biopsy cores were calculated. For side-specific evaluation of the specimens, the prostates were visually divided bilaterally (right and left sides). Then the extent of side-specific prostatic capsular invasion on each side was measured. Results were divided into two categories: ECE side and non-ECE side (i.e. side with no cancer focus). The non-ECE side was subclassified into a capsular contact side, in which the tumor was confined to the prostate within a layer more fibrous than muscular (capsule),[9] and a non-capsular contact or no cancer side.

Clinical cancer staging and evaluation of prostatic capsular invasion levels

Cancer stage was assigned on the basis of the 2009 Union for International Cancer Control 7th TNM staging system.[10] Conventional T1/T2WI and DWI MRI was carried out using a clinical 3.0-T MRI system (Magnetom Trio with TIM system; Siemens, Erlangen, Germany) and a standard body coil. *B*-values of DWI were 0–1500 s/mm^2. MRI was carried out preoperatively over a period of 4 weeks after biopsy. MRI images were preoperatively assessed by two radiologists (TM and MM). The findings of T2WI were evaluated for cancer location and visually categorized as follows: unremarkable, organ-confined cancer without capsular contact, cancer with capsular contact and ECE cancer. A cancer focus with ECE on T2WI MRI was defined as T2WI MRI-positive. The slice thickness of our 3.0-T MRI T2WI was 0.73 mm. Therefore, the detection of microscopic ECE (<1 mm) was difficult using MRI. We referenced the previously reported criteria to predict the microscopic ECE by MRI findings, which consisted of the disruption of the prostatic capsule, extension into the periprostatic fat, broad contact with the capsule (>12 mm), irregular capsular bulge, obliteration of the rectoprostatic angle and neurovascular bundle involvement.[11] The findings of DWI MRI were visually categorized as follows: unremarkable, confined to the prostate without capsular contact and capsular contact or ECE cancer. The last was a dual category, because it was difficult to clearly distinguish the ECE side with DWI MRI alone. A cancer focus with capsular contact or ECE on DWI MRI was defined as DWI MRI-positive. When evaluation of cancer location was difficult because of residual bleeding caused by biopsy or measurement artifacts, MRI T2WI and DWI findings were judged to be unremarkable. Clinical TNM staging was determined using a combination of DRE, TRUS and MRI information.

Methods of analysis

In the primary study sample, the association of side-specific ECE with clinical and biopsy features was assessed using the Wilcoxon rank-sum test with continuity correction and Fisher's exact test. The variables, including serum PSA level, biopsy Gleason score, DRE, TRUS, the number of positive biopsy cores on each side, the maximum percentage of positive cores on each side, T2WI MRI findings, and DWI MRI findings were tested using univariate and multivariate logistic regression analyses to evaluate their association with side-specific ECE. The optimal cut-off values maximizing the sum of sensitivity plus specificity were statistically determined for the univariate analyses. Multivariate logistic regression analyses used backward, stepwise selection for variables with $P < 0.1$ in the univariate analyses, and the variable remained if the significance level was $P < 0.05$ for that variable. Statistically significant factors ($P < 0.05$) according to multivariate logistic regression analysis were used to construct a model for the prediction of side-specific ECE. The predictive accuracy for the model was quantified by measuring sensitivity, specificity, PPV, NPV, diagnostic accuracy and OR. The accuracy of the constructed prediction model for the determination of side-specific ECE was validated using the validation study sample. A flowchart was then constructed on the basis of the prediction model for both study samples. All statistical analyses were carried out using the freely downloadable *R* statistical software v2.13.0 (http://cran.r-project.org).[12]

Results

Bilateral and unilateral nerve-sparing RP was carried out in four (3.0%) and 18 (13.6%) of the 132 patients in the

Table 1 Clinical and pathological characteristics in the primary and validation study samples

	Primary study set (132 patients)	Validation study set (134 patients)
Variables		
Median age, years (range)	65.5 (51–78)	65 (50–81)
Median serum PSA value (range)	8.5 (2.2–67.0)	7.9 (3.3–57.9)
Biopsy Gleason score; *n* (%)		
6 or less	10 (7.6)	9 (6.7)
3 + 4	59 (44.7)	52 (38.8)
4 + 3	49 (37.1)	53 (39.6)
8 or greater	14 (10.6)	20 (14.9)
Clinical T stage; *n* (%)		
T1c	9 (6.8)	12 (9.0)
T2a/b	44 (33.3)	65 (48.5)
T2c	37 (28.0)	28 (20.9)
T3a	42 (31.8)	29 (21.6)
Pathological T stage; *n* (%)		
pT2a/b	22 (16.7)	24 (17.9)
pT2c	48 (36.4)	57 (42.5)
pT3a	47 (35.6)	43 (32.1)
pT3b	15 (11.4)	10 (7.5)
Pathological capsular invasion extent in each lobe		
Non-ECE		
No capsular contact + no cancer focus	62 (23.5)	67 (25.0)
Capsular contact	131 (49.6)	140 (52.2)
ECE	71 (26.9)	61 (22.8)

primary sample, and two (1.5%) and 25 (18.7%) of the 134 patients in the validation sample, respectively. All surgical margins were negative on the nerve-sparing sides. Therefore, these sides were included in the analysis. The clinical and pathological features of the study samples are shown in Table 1. Neither positive imaging nor significant DRE findings were found in nine (6.8%) and 12 (9.0%) of the T1c patients in the primary and validation samples, respectively. The well-developed and extended prostatectomy technique used in our institution was used for all high-risk and relatively high-risk patients.[13] Therefore, pathologically confirmed side-specific ECE cancer was identified in 71 (26.9%) of the 264 sides examined in the primary sample, and 61 (22.8%) of the 268 sides examined in the validation sample, respectively.

Results of the side-specific analysis of specimens in the primary sample, as well as data regarding pathologically confirmed capsular invasion and its association with clinical and pathological features, are shown in Table 2. Although MRI findings were judged to be unremarkable in cases that were difficult to evaluate because of residual bleeding or the measurement artifacts, the number of such cases was few (less than 5% of the total). In the analysis of the primary sample, the optimal cut-off values were determined as follows: biopsy Gleason score = 8, serum PSA level = 10.1 ng/mL, number of positive biopsy cores on each side = 2 and maximum percentage of cores positive for cancer on each side = 31%. In the univariate analysis, serum PSA level, biopsy Gleason score ≥8, ≥2 positive biopsy cores on each side, maximum percentage of cores positive for cancer on each side ≥31%, positive DWI MRI findings and positive T2WI MRI findings were significant predictors ($P < 0.05$) of side-specific ECE in the surgical specimens (Table 3). Results for TRUS for each side were almost significant ($P < 0.1$). Multivariate analysis with stepwise selection showed biopsy Gleason scores of ≥8 ($P < 0.005$), DWI MRI-positivity ($P < 0.01$), ≥2 positive biopsy cores on each side ($P < 0.05$) and maximum percentage of cores positive for cancer on each side ≥31% ($P < 0.05$) as significant independent predictors ($P < 0.05$) of side-specific ECE (Table 3). Figure 1 shows representative 3.0-T MRI findings. The predictive accuracy based on each factor is summarized in Table 4. When a combination prediction model was run using any of the four significant predictors (3 biopsy factors in combination with positive DWI MRI findings), 67 of 71 pathologically confirmed ECE sides were correctly predicted in the primary sample (sensitivity 94.4%; 95% CI 86.2–98.4). In addition, four of 66 negatively predicted sides were pathologically determined to have ECE (NPV 93.9%; 95% CI 85.2–98.3%). In the validation sample, the sensitiv-

Table 2 Association of pathologically confirmed prostatic capsular invasion in each lobe with preoperative clinicopathological features in the primary sample

Factors	No. lobes, *n* (%)			
Pathological extent of prostatic capsular invasion	Non-ECE		ECE	Total
	No capsular contact	Capsular contact		
Total no. each lobes	62	131	71	264
Serum PSA value				
Less than 4.0	4 (6.5)	5 (3.8)	1 (1.4)	10 (3.8)
4.1–10.0	39 (62.9)	80 (61.1)	33 (46.5)	152 (57.6)
10.1–20.0	14 (22.6)	31 (23.7)	23 (32.4)	68 (25.8)
≥20.1	5 (8.1)	15 (11.5)	14 (19.7)	34 (12.9)
DRE findings for each side				
Non-palpable	48 (77.4)	93 (71.0)	47 (66.2)	188 (71.2)
Palpable	14 (22.6)	38 (29.0)	24 (33.8)	76 (28.8)
TRUS findings for each side				
Unremarkable	44 (71.0)	85 (64.9)	39 (54.9)	168 (63.6)
Echogenic	18 (29.0)	46 (35.1)	32 (45.1)	96 (36.4)
Biopsy Gleason score/patient				
6 or less	5 (8.1)	11 (8.4)	4 (5.6)	20 (7.6)
3 + 4	23 (37.1)	73 (55.7)	22 (31.0)	118 (44.7)
4 + 3	27 (43.5)	43 (32.8)	28 (39.4)	98 (37.1)
≥8	7 (11.3)	4 (3.1)	17 (23.9)	28 (10.6)
Biopsy results for each side				
No. positive cores				
0	34 (54.8)	20 (15.3)	7 (9.9)	61 (23.1)
1	17 (27.4)	32 (24.4)	9 (12.7)	58 (22.0)
2	7 (11.3)	23 (17.6)	15 (21.1)	45 (17.0)
≥3	4 (6.5)	56 (42.7)	40 (56.3)	100 (37.9)
Maximum percentage of positive cores on each side				
0%	34 (54.8)	20 (15.3)	7 (9.9)	61 (23.1)
1–10%	15 (24.2)	25 (19.1)	10 (14.1)	50 (18.9)
11–30%	11 (17.7)	49 (37.4)	9 (12.7)	69 (26.1)
31–50%	1 (1.6)	11 (8.4)	19 (26.8)	31 (11.8)
51–100%	1 (1.6)	26 (19.8)	26 (36.6)	53 (20.1)
MRI judgments on each side				
T2WI MRI				
Unremarkable	39 (62.9)	38 (29.0)	7 (9.9)	84 (31.8)
Confined cancer without capsular contact	11 (17.7)	19 (14.5)	11 (15.5)	41 (15.5)
Capsular contact	11 (17.7)	52 (39.7)	27 (38.0)	90 (34.1)
ECE (T2WI MRI positive)	1 (1.6)	22 (16.8)	26 (36.6)	49 (18.6)
DWI MRI				
Unremarkable	41 (66.1)	44 (33.6)	14 (19.7)	99 (37.5)
Confined cancer without capsular contact	12 (19.4)	15 (11.5)	6 (8.5)	33 (12.5)
Capsular contact or ECE (DWI MRI-positive)	9 (14.5)	72 (55.0)	51 (71.8)	132 (50.0)

ity, specificity, PPV and NPV of ECE prediction using the proposed model were 93.4% (57/61; 95% CI 84.1–98.2%), 27.5% (57/207; 95% CI 21.6–34.2%), 27.5% (57/207; 95% CI 21.6–34.2%), and 93.4% (57/61; 95% CI 84.1–98.2%), respectively. Therefore, the analysis of the validation sample showed the model to have good reproducibility.

Figure 2 shows a flowchart including all 532 sides categorized using a combination of biopsy information and DWI MRI findings. In total, 94, 111 and 124 of 132 pathologically confirmed ECE cases were correctly predicted using DWI MRI alone, a combination of the three biopsy factors and our prediction model, respectively (sensitivity, 71.2%, 84.1 and 93.9%, respectively). Pathologically confirmed ECE was misdiagnosed by DWI MRI alone in 14.3% patients (38/266), a combination of the three biopsy factors in 11.2% patients (21/188) and our prediction model in

Table 3 Factors predicting pathologically confirmed side-specific extracapsular extension according to univariate and multivariate logistic regression analyses

	Univariate analysis	Multivariate logistic regression analysis	
	P-value	OR (95% CI)	*P*-value
Variables			
Continuous PSA value†	<0.001	1.02 (0.99–1.05)	0.23
≤10.0 ng/mL *vs* ≥10.1 ng/mL	<0.01		
Biopsy Gleason score			
≤7 *vs* ≥8	<0.001	5.66 (2.28–14.0)¶	<0.005
DRE on each side			
Non-palpable *vs* palpable	0.29		
TRUS on each side			
Unremarkable *vs* echogenic	0.08	0.75 (0.38–1.48)	0.41
No. positive biopsy cores on each side			
≤1 *vs* ≥2	<0.001	2.22 (1.05–4.70)¶	<0.05
Maximum percentage of positive cores on each side			
≤30% *vs* ≥31%	<0.001	2.16 (1.07–4.37)¶	<0.05
T2WI MRI			
Negative *vs* positive‡	<0.001	1.78 (0.80–3.94)	0.16
DWI MRI			
Negative *vs* positive§	<0.001	2.39 (1.26–4.54)¶	<0.01

†Wilcoxon rank-sum test with continuity correction. ‡A cancer focus with ECE on T2WI MRI was defined as T2WI MRI positive. §A cancer focus with capsular contact or ECE on DWI MRI was defined as DWI MRI positive. ¶These factors were statistically significant in the final model, and the OR of the final model are shown.

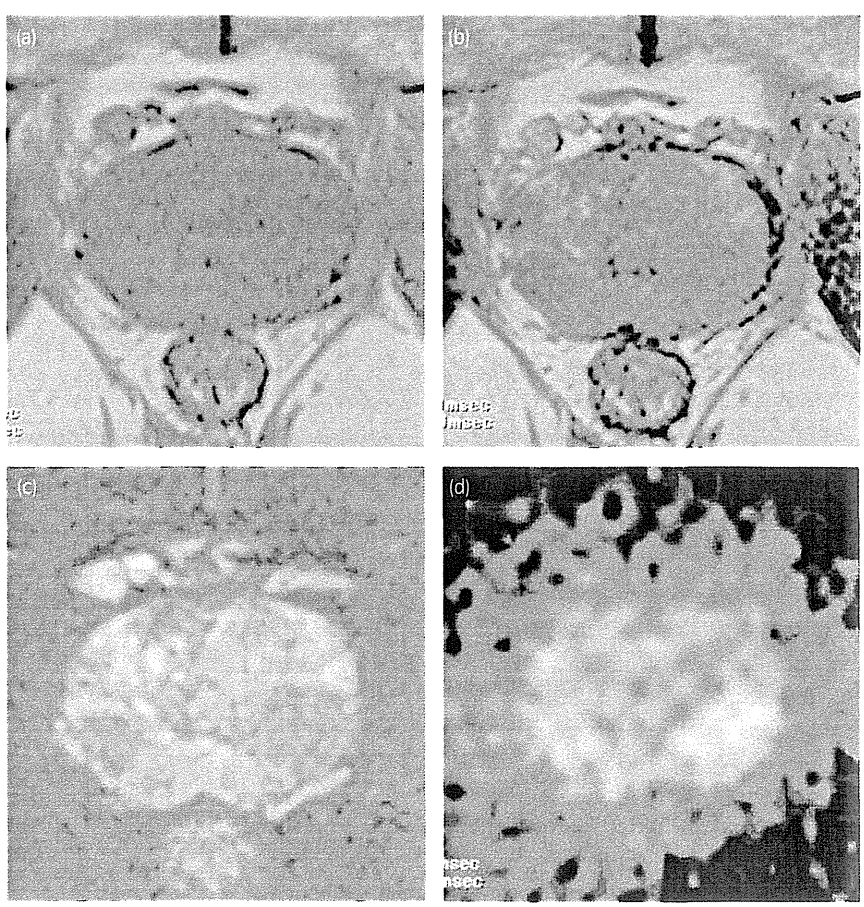

Fig. 1 Representative data of a prostate cancer patient shows the pathological ECE cancer in the peripheral zone of the left lobe and the capsular contact cancer in the peripheral zone of the right lobe. (a) There is no residual intraprostatic bleeding caused by biopsy on T1WI MRI. (b) T2WI MRI and (c) T2WI MRI with fat suppression show the ECE cancer focus in the left lobe and the capsular contact cancer focus in the right lobe. (d) DWI MRI shows a positive cancer focus on both sides.

Table 4 Performance characteristics predicting pathologically confirmed side-specific ECE in the primary sample (264 lobes)

	Sensitivity (%) (95% CI)	Specificity (%) (95% CI)	PPV (%) (95% CI)	NPV (%) (95% CI)	Diagnostic accuracy (%) (95% CI)	Odds ratio
Predictors for pathological ECE cancer						
Biopsy Gleason score ≥8	23.9 (17/71) (14.6–35.5)	94.3 (182/193) (90.0–97.1)	60.7 (17/28) (40.6–78.5)	77.1 (182/236) (71.2–82.3)	75.4 (69.7–80.5)	5.17 (2.14–13.0)
DWI MRI-positive	71.8 (51/71) (59.9–81.9)	58.0 (112/193) (50.7–65.1)	38.6 (51/132) (30.3–47.5)	84.8 (112/132) (77.6–90.5)	61.7 (55.6–67.6)	3.51 (1.89–6.72)
Positive biopsy cores ≥2 on each side	77.5 (55/71) (66.0–86.5)	53.4 (103/193) (46.1–60.6)	37.9 (55/145) (30.0–46.4)	86.6 (103/119) (79.1–92.1)	59.8 (53.7–65.8)	3.91 (2.04–7.86)
Maximum percentage of positive cores ≥31% on each side	52.1 (37/71) (39.9–64.1)	75.6 (146/193) (69.0–81.5)	44.0 (37/84) (33.2–55.3)	81.1 (146/180) (74.6–86.5)	69.3 (63.4–74.8)	3.36 (1.83–6.21)
Combination prediction model†	94.4 (67/71) (86.2.5–98.4)	32.1 (62/193) (25.6–39.2)	33.8 (67/198) (27.3–40.9)	93.9 (62/66) (85.2 × 98.3)	48.9 (42.7–55.1)	7.88 (2.75–31.1)

†In combination with biopsy Gleason score ≥8, DWI MRI positivity, positive biopsy cores ≥2 on either side, or maximum percentage of positive cores ≥31% on either side.

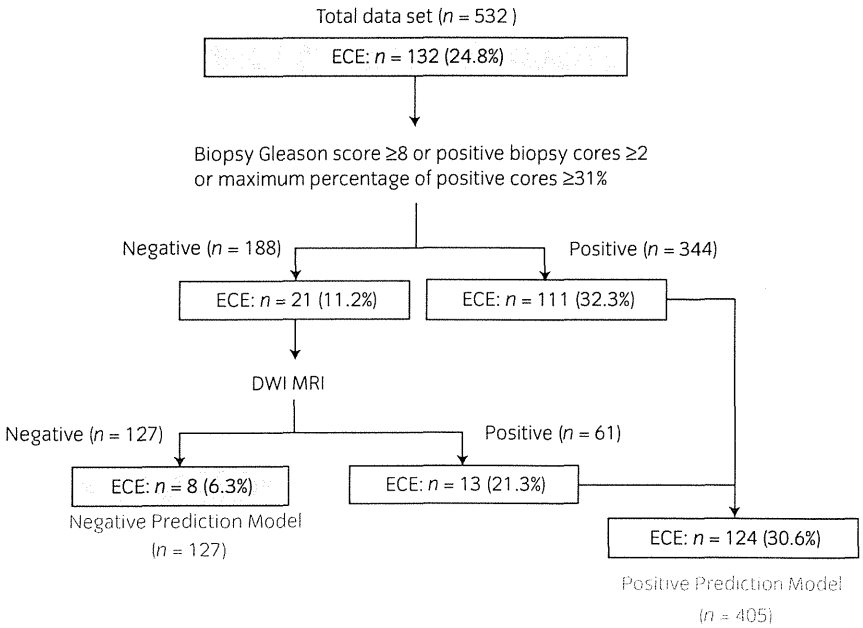

Fig. 2 Flowchart beginning with 532 prostate sides in the total study sample (□). A positive prediction model for ECE is shown (□) through a combination of biopsy information and 3.0-T DWI MRI. A negative prediction model is also shown (□).

6.3% patients (8/127; NPV 85.7%, 88.8% and 93.7%, respectively). OR were 3.27 (95% CI 2.10–5.16), 3.78 (95% CI 2.25–6.62) and 6.55 (95% CI 3.09–16.0) for DWI MRI alone, a combination of the three biopsy factors and our prediction model, respectively. Therefore, sensitivity (93.9% *vs* 84.1%) and NPV (93.7% *vs* 88.8%) were higher for the prediction model than for the combination of the three biopsy factors. Additional DWI MRI information correctly predicted 13 (61.9%) of 21 pathologically confirmed ECE sides that were incorrectly predicted by a combination of the three biopsy factors. However, the specificity (29.8%) and PPV (30.6%) of our prediction model were low.

Discussion

Recent studies have shown improvements in prostate cancer diagnosis with the use of 3.0-T MRI, including DWI.[1] Several studies have also shown the usefulness of T2WI MRI in combination with DWI MRI for improving cancer detection.[3,4,14,15] In one study, cancer detection by T2WI in the TZ

was reportedly inferior to that in the PZ.[13] DWI improved cancer detection rate in the TZ, although DWI sensitivity for cancer in TZ was still lower than that in PZ.[14] Other recently published reports have shown a significant correlation between DWI/ADC values and cancer cell density, Gleason grade, and D'Amico clinical risk scores.[12,14] Well-differentiated cancers of predominant glandular composition yield relatively higher ADC values.[14] In our series, cancer lesions evaluated with 3.0-T DWI MRI imaging were positively associated with high Gleason score, TZ location and higher cancer volume. In contrast, small lesions (<5 mm in diameter) were frequently missed in prostatectomy specimens (data not shown). Therefore, 3.0-T DWI MRI might be useful in predicting the aggressiveness of prostate cancer.

In the current study, the 12-core-biopsy technique and pathological analysis were standard procedures for patients in the primary sample. The results using the model constructed on the basis of data from the primary sample were reproducible in the validation sample. This model predicted side-specific ECE with high sensitivity (93.9%) and NPV (93.7%) compared with conventional biopsy information alone. However, specificity (29.8%) and PPV (30.6%) were low. Our model was useful in the evaluation of non-ECE sides, but just 23.9% patients fit the model. Therefore, the proposed model was reliable only for predicting non-ECE sides. Other limitations included the retrospective nature of the study and sample selection bias. Prostatectomy is carried out at our institution for high-risk and relatively high-risk prostate cancer patients.[13] Therefore, the percentage of patients with clinical stage T3a cancer was higher than that seen at other institutions. In addition, MRI images were evaluated subjectively by two radiologists, and PPV for cancer detection using 3.0-T DWI MRI alone was still low because of the low image resolution.

In conclusion, the present study identified the correlation of conventional preoperative features and 3.0-T DWI MRI with side-specific ECE detection in prostatectomy specimens. 3.0-T DWI MRI evaluation was an independent variable that significantly predicted side-specific ECE. The findings of 3.0-T DWI MRI combined with the evaluation of conventional preoperative features might assist in predicting side-specific non-ECE. Our ECE prediction model that uses the biopsy Gleason score and factors associated with tumor location (DWI MRI positivity, positive biopsy core and maximum percentage of positive cores) has a high NPV, but a low PPV. Nevertheless, it was reproducible in a validation sample; therefore, it might be useful for predicting non-ECE sides.

Acknowledgments

This study was supported by grants from the Ministry of Health and Welfare for the Third-term Comprehensive 10-year Strategy for Cancer Control.

Conflict of interest

None declared.

References

1 Dickinson L, Ahmed HU, Allen C *et al.* Magnetic resonance imaging for the detection, localisation, and characterisation of prostate cancer: recommendations from a European Consensus Meeting. *Eur. Urol.* 2011; **59**: 477–94.
2 Zelhof B, Pickles M, Liney G *et al.* Correlation of diffusion-weighted magnetic resonance data with cellularity in prostate cancer. *BJU Int.* 2009; **103**: 883–8.
3 Nishida S, Kinoshita H, Mishima T, Kurokawa H, Sakaida N, Matsuda T. Prostate cancer detection by prebiopsy 3.0-Tesla magnetic resonance imaging. *Int. J. Urol.* 2011; **18**: 653–8.
4 Jeong IG, Kim JK, Cho KS *et al.* Diffusion-weighted magnetic resonance imaging in patients with unilateral prostate cancer on extended prostate biopsy: predictive accuracy of laterality and implications for hemi-ablative therapy. *J. Urol.* 2010; **184**: 1963–9.
5 Ohori M, Kattan MW, Koh H *et al.* Predicting the presence and side of extracapsular extension: a nomogram for staging prostate cancer. *J. Urol.* 2004; **171**: 1844–9.
6 Kupelian PA, Katcher J, Levin HS, Klein EA. State T1-2 prostate cancer: a multivariate analysis of factors affecting biochemical and clinical failures after radical prostatectomy. *Int. J. Radiat. Oncol. Biol. Phys.* 1997; **37**: 1043–52.
7 Graefen M, Walz J, Huland H. Open retropubic nerve-sparing radical prostatectomy. *Eur. Urol.* 2006; **49**: 38–48.
8 Gontero P, Kirby RS. Nerve-sparing radical retropubic prostatectomy: techniques and clinical considerations. *Prostate Cancer Prostatic Dis.* 2005; **8**: 133–9.
9 Wheeler TM, Dillioglugil O, Kattan MW *et al.* Clinical and pathological significance of the level and extent of capsular invasion in clinical stage T1-2 prostate cancer. *Hum. Pathol.* 1998; **29**: 856–62.
10 Sobin LH, Gospodarowicz MK, Wittekind CH (eds) *TNM Classification of Malignant Tumors UICC International Union Against Cancer*, 7th edn. Wiley-Blackwell, New York, 2009; 243–8.
11 Bloch BN, Furman-Haran E, Helbich TH *et al.* Prostate cancer: accurate determination of extracapsular extension with high-spatial-resolution dynamic contrast-enhanced and T2-weighted MR imaging – initial results1. *Radiology* 2007; **245**: 176–85.
12 Team RDC. *R: A Language and Environment for Statistical Computing*. R Foundation for Statistical Computing, Vienna, Austria, 2011.
13 Miyake H, Fujimoto H, Komiyama M, Fujisawa M. Development of "extended radical retropubic prostatectomy": a surgical technique for improving margin positive rates in prostate cancer. *Eur. J. Surg. Oncol.* 2010; **36**: 281–6.
14 Tan C, Wang J, Kundra V. Diffusion weighted imaging in prostate cancer. *Eur. Radiol.* 2011; **21**: 593–603.
15 Haider MA, van der Kwast TH, Tanguay J *et al.* Combined T2-weighted and diffusion-weighted MRI for localization of prostate cancer. *AJR Am. J. Roentgenol.* 2007; **189**: 323–8.

Identification of HLA-A2 or HLA-A24-restricted CTL epitopes for potential HSP105-targeted immunotherapy in colorectal cancer

YU SAWADA[1,2*], HIROYUKI KOMORI[3,4*], YOSHIYUKI TSUNODA[1,5,6*], MANAMI SHIMOMURA[1], MARI TAKAHASHI[1], HIDEO BABA[4], MASAAKI ITO[5], NORIO SAITO[5], HIROYUKI KUWANO[6], ITARU ENDO[2], YASUHARU NISHIMURA[3] and TETSUYA NAKATSURA[1]

[1]Division of Cancer Immunotherapy, Exploratory Oncology Research and Clinical Trial Center, National Cancer Center, Kashiwa 277-8577; [2]Department of Gastroenterological Surgery, Yokohama City University Graduate School of Medicine, Yokohama 236-0004; Departments of [3]Immunogenetics and [4]Gastroenterological Surgery, Graduate School of Medical Sciences, Kumamoto University, Kumamoto 860-8556; [5]Colorectal and Pelvic Surgery Division, National Cancer Center Hospital East, Kashiwa 277-8577; [6]Department of General Surgical Science (Surgery I), Gunma University Graduate School of Medicine, Maebashi 371-8511, Japan

Received October 21, 2013; Accepted November 25, 2013

DOI: 10.3892/or.2013.2941

Abstract. We previously reported that heat shock protein 105 (HSP105) is overexpressed in a variety of human cancers, including colorectal, pancreatic and esophageal cancer and has proven to be a novel biomarker for the immunohistochemical detection of these cancers. In the present study, we used HLA-transgenic mice (Tgm) and the peripheral blood mononuclear cells (PBMCs) of colorectal cancer patients to identify HLA-A2 and HLA-A24-restricted HSP105 epitopes, as a means of expanding the application of HSP105-based immunotherapy to HLA-A2- or HLA-A24-positive cancer patients. In addition, we investigated by *ex vivo* IFN-γ ELISPOT assay whether the HSP105-derived peptide of cytotoxic T cells (CTLs) exists in PBMCs of pre-surgical colorectal cancer patients. We found that four peptides, HSP105 A2-7 (RLMNDMTAV), HSP105 A2-12 (KLMSSNSTDL), HSP105 A24-1 (NYGIYKQDL) and HSP105 A24-7 (EYVYEFRDKL), are potential HLA-A2 or HLA-A24-restricted CTL HSP105-derived epitopes. HSP105-specific IFN-γ-secreting T cells were detected in 14 of 21 pre-surgical patients with colorectal cancer in response to stimulation with these four peptides. Our study raises the possibility that these HSP105 peptides are applicable to cancer immunotherapy in patients with HSP105-expressing cancer, particularly colorectal cancer.

Correspondence to: Dr Tetsuya Nakatsura, Division of Cancer Immunotherapy, Exploratory Oncology Research and Clinical Trial Center, National Cancer Center, 6-5-1 Kashiwanoha, Kashiwa 277-8577, Japan
E-mail: tnakatsu@east.ncc.go.jp

*Contributed equally

Key words: cancer immunotherapy, cytotoxic T cell, colorectal cancer, heat shock protein 105, HLA-transgenic mice

Introduction

Colorectal cancer is one of the most prevalent cancers and a major cause of mortality worldwide (1). Although adjuvant systemic chemotherapy or chemoradiation can confer a limited but significant survival advantage, novel and more effective therapies are needed. To improve survival rates, new therapeutic agents have been investigated. Immunotherapy for colorectal cancer is a promising candidate treatment, and there is evidence that host immune responses can influence survival (2). Ideal targets for immunotherapy are gene products overexpressed in cancer cells but silenced in normal tissues, with the exception of immune-privileged tissues, such as that of the testis.

We previously reported that heat shock protein 105 (HSP105), identified by SEREX, is overexpressed in a variety of human cancers, including colorectal, pancreatic and esophageal cancer, but with little to no expression in normal tissues aside from the testis (3,4). HSP105 is a stress protein induced by various stressors and belongs to the HSP105/110 family and plays an important role as a chaperone under physiological conditions (5). Using immunohistochemical analysis, we previously found that HSP105 was specifically overexpressed in 44 of 53 (83.0%) colorectal cancer patients (4). It has also been reported that DNA vaccination with both HSP105 and bone marrow-derived dendritic cells (BM-DCs) pulsed with HSP105 led to tumor rejection of colorectal cancer but did not induce an autoimmune reaction in mice (6-8).

This suggests that HSP105 presents a useful tumor-specific antigen target for immunotherapy. However, HSP105-derived epitope peptides of $CD8^+$ T cells have not been identified. The gene frequency of HLA-A24 (A*24:02) is relatively high in Asian populations, especially the Japanese, but low in Caucasians. On the other hand, the gene frequency of HLA-A2 (A*02:01) is high among several ethnic groups, including Asians and Caucasians (9). Therefore, HLA-A2 or HLA-A24-restricted cytotoxic T cell (CTL) HSP105 epitopes could be extremely

useful for immunotherapy in a large portion of patients worldwide. In the present study, we identified human HSP105-derived CTL epitopes restricted by HLA-A2 or HLA-A24 using HLA-transgenic mice (Tgm) and examined whether these epitope-based peptides could activate HSP105-reactive CTLs in peripheral blood mononuclear cells (PBMCs) of patients with colorectal cancer.

Materials and methods

Mice. HLA-A2.1 (HHD) Tgm, H-2D$^{b-/-}$β2m$^{-/-}$ double-knockout mice introduced with the human β2m-HLA-A2.1(α1 α2)-H-2D^{b} (α3 transmembrane cytoplasmic) (HHD) mono-chain gene construct were generated in the Departmente SIDA-Retrovirus, Unite d' Immunite Cellulaire Antivirale, Institut Pasteur, Paris, France (10,11) and were kindly provided by Dr F.A. Lemonier. HLA-A24.2 (HHD) Tgm were purchased from Japan SLC, Inc. (Shizuoka, Japan). Female 6- to 8-week-old BALB/c mice (H-2K^{d}) and BALB/c nude mice, purchased from Charles River Japan (Yokohama, Japan), were maintained and handled in accordance with animal care policy.

Cell lines. The human colorectal cancer cell line SW620 (endogenously expressing HSP105 and HLA-A*02:01, 24:02) and human liver cancer cell line HepG2 (HSP105-low expressing and HLA-A*02:01, 24:02), were kindly provided by the Cell Resource Center for Biomedical Research, Institute of Development, Aging and Cancer (Tohoku University, Sendai, Japan). Murine colorectal cancer cells, Colon26 (C26) (endogenously expressing HSP105 and H-2K^{d}) were kindly provided by Dr Kyoichi Shimomura (Fujisawa Pharmaceutical Co., Osaka, Japan). T2 cells (a TAP-deficient and HLA-A*02:01-positive cell line) were provided by Kyogo Ito of Kurume University. Cells were maintained *in vitro* in RPMI-1640 or DMEM supplemented with 10% FCS.

RNA interference. Small interfering RNAs targeting human HSP105 were chemically synthesized by Dharmacon Research (HSP105-siRNA and luciferase; Lafayette, CO, USA) as previously described (12), with the following siRNA sequences: HSP105-siRNA, UUGGCUGCAACUCCGAUU GTT and luciferase, CGUACGCGGAAUACUUCGATT. The transfection of siRNA oligonucleotides was carried out using Oligofectamine (Invitrogen, Carlsbad, CA, USA) according to the manufacturer's guidelines.

Peptides. Human HSP105-derived peptides, identical in amino acid sequence with mouse HSP105 and expressing the binding motifs for HLA-A*02:01- and HLA-A*24:02-encoded molecules, were designed with BIMAS software (BioInformatics and Molecular Analysis Section; Center for Information Technology, NIH, MD, USA). We purchased a total of 16 versions of peptides carrying the HLA-A2 (A*0201)-binding motifs and 9 versions of peptides carrying the HLA-A24 (A*2402)-binding motifs from Biologica (Tokyo, Japan) (Table I).

Induction of HSP105-reactive CTLs in Tgm. Peptide immunizations in mice were performed as previously described (13). In brief, bone marrow (BM) cells (2x10^{6}) from HLA-A2 or HLA-A24 Tgm were cultured in RPMI-1640 medium supplemented with 10% FCS, GM-CSF (5 ng/ml) and 2-mercaptoethanol (0.8 ng/ml) for 7 days in 10-cm plastic dishes. These BM-DCs were pulsed with the two HSP105 peptide mixtures (1 μmol/l each peptide) for 2 h at 37°C. We primed the HLA-A2 or HLA-A24 Tgm with the syngeneic BM-DC vaccine (5x10^{5}/mice) into the peritoneal cavity twice, once per week. Seven days following the last immunization, the spleens were collected and CD4^{-} spleen cells were isolated by negative selection with anti-CD4 microbeads (Miltenyi Biotec, Bergisch Gladbach, Germany) to exclude any nonspecific IFN-γ production from the CD4^{+} spleen cells co-cultured with the BM-DCs. The CD4^{-} spleen cells (2x10^{6}/well) were stimulated with syngeneic BM-DCs (2x10^{5}/well) that had been pulsed with each peptide *in vitro*. After 6 days, the frequency of cells producing IFN-γ/2x10^{4} CD4^{-} spleen cells upon stimulation with syngeneic BM-DCs (1x10^{4}/well), pulsed with or without each peptide, was assayed using an enzyme-linked immunospot (ELISPOT) assay as previously described (13).

Identification of a CTL epitope in BALB/c mice. The peptide immunizations in mice were performed as previously described (14). Splenocytes removed from mice 7 days following the last immunization were harvested and cultured in 24-well culture plates (2.5x10^{6}/well) in 45% RPMI, 45% AIMV, 10% FCS and supplemented with recombinant human interleukin 2 (100 U/ml), 2-mercaptoethanol (50 μmol/l) and each peptide (10 μmol/l). After 5 days, the cytotoxicity of these cells against target cells was assayed using standard 6-h ^{51}Cr release assays (15).

Blood samples. Blood samples from cancer patients were collected during routine diagnostic procedures after obtaining formal consent from patients at the Kumamoto University Hospital, from April to September 2006 and from patients at the National Cancer Center Hospital East, from December 2006 to March 2007. The study was approved by the local ethics committee, and informed consent was obtained from all patients.

Induction of HSP105-reactive human CTLs. We isolated PBMCs from heparinized blood of HLA-A24^{+} and/or HLA-A2^{+} Japanese patients with colorectal cancer using Ficoll-Conray density gradient centrifugation; peripheral monocyte-derived dendritic cells (DCs) were generated as previously described (16,17). CD8^{+} T cells were isolated with CD8 microbeads (Miltenyl Biotec, Bergisch Gladbach, Germany) from PBMCs of the same donor and peptide-reactive CD8^{+} CTLs were generated. Five days following the last stimulation, the cytotoxic activities of the CTLs against cancer cell lines were measured by ^{51}Cr-release assay as previously described (15). For these assays, CTLs were co-cultured with each cancer cell line, as the target cells (5x10^{3}/well), at the indicated effector/target ratio.

In vivo tumor challenge. Subcutaneous tumors were induced in mice by injecting 1x10^{4} SW620 cells suspended in 100 μl PBS or Hanks' balanced salt solution (Gibco, Grand Island, NY, USA) into the backs of BALB/c nude mice. Tumor incidence and volumes were assessed weekly using calipers and tumor areas were measured. Results are presented as mean tumor areas ± SD.

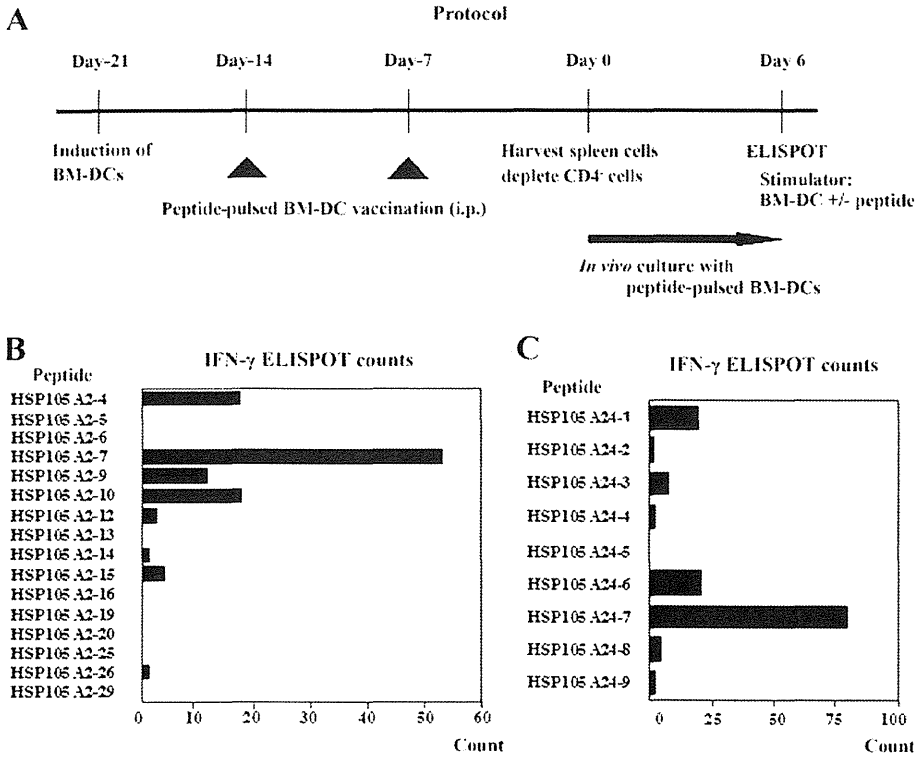

Figure 1. Identification of HLA-A2 or HLA-A24-restricted CTL epitopes of HSP105 using HLA-A2.1 Tgm and HLA-A24 Tgm. (A) The protocol used for identification of HLA-A2 or HLA-A24-restricted CTL epitopes of HSP105 is shown. We primed the HLA Tgm with BM-DCs ($5x10^5$) pulsed with the mixture of HSP105-derived peptides carrying the HLA-A2 or HLA-A24 binding motif into the peritoneal cavity once a week for 2 weeks. Seven days after the last DC vaccination, spleens were collected and $CD4^-$ spleen cells ($2x10^6$/well) were stimulated with syngeneic BM-DCs ($2x10^5$/well) pulsed with each peptide *in vitro* for 6 days. We used these cultured $CD4^-$ spleen cells as responder cells in the IFN-γ ELISPOT assay. (B) The bar graphs show the IFN-γ ELISPOT counts per $2x10^4$ $CD4^-$ spleen cells co-cultured with HLA-A2-restricted peptide-pulsed BM-DCs after normalization to counts from cells co-cultured with BM-DCs without peptide loading. (C) The bar graphs show the IFN-γ ELISPOT counts in the HLA-A24-restricted peptides. The columns represent the means from duplicate assays.

Ex vivo IFN-γ ELISPOT assay in peripheral blood in pre-surgical colorectal cancer patients. Ex vivo IFN-γ ELISPOT assays were performed to determine tumor-specific interferon-γ (IFN-γ)-secreting T cells. The 96-well plates were coated with anti-human IFN-γ (BD Biosciences Co., Ltd., USA). After an overnight incubation at 4°C, the wells were washed and blocked with complete medium for 2 h at room temperature. A total of $1x10^6$ unfractionated PBMCs were added in duplicate wells and incubated at 37°C for 18-20 h with or without peptides at 0.2 μl/well (1-10 μM). The plate was washed and then incubated with 5 μg/ml biotinylated anti-human IFN-γ antibody for 2 h at room temperature. After washing away the antibodies, streptavidin-HRP was added for 1 h. Finally, the plate was washed and replaced with fresh substrate solution and the reaction was terminated by washing with distilled water. The HLA-A2-restricted CMV peptide (NLVPMVATV) and HLA-A24 restricted CMV peptide (QYDPVAALF), which includes an epitope derived from the CMV pp65 protein, were used as positive controls.

Histological and immunohistochemical analysis. To investigate whether $CD8^+$ T cells infiltrated normal tissues triggered by the HSP105-derived peptide vaccine, we performed immunohistochemical staining with a monoclonal antibody against CD8 (1:100; LifeSpan BioSciences, Inc., Seattle, WA, USA) in tissue specimens from HLA-A2 Tgm immunized with the HSP105 peptides, as previously described (7). Immunohistochemical staining with rabbit polyclonal antibodies against HSP105 (1:200; Santa Cruz Biotechnology, Inc.; Santa Cruz, CA, USA) was performed according to the manufacturer's instructions.

Results

Identification of HLA-A2-or HLA-A24-restricted CTL epitopes in HLA Tgm. We designed pools of HSP105 peptides possessing amino acid sequences conserved between humans and mice that have a highly predicted binding score to HLA-A2 (pool of 16 different peptides) or HLA-A24 (A*24:02) (pool of 9 different peptides) (Table I). $CD4^-$ spleen cells were obtained from Tgm immunized twice i.p. with BM-DCs that had been pulsed with each peptide mixture; the spleen cells were then stimulated *in vitro*, again with the BM-DCs pulsed with each peptide mixture (Fig. 1A).

The IFN-γ ELISPOT counts, normalized to those of spleen cells co-cultured with BM-DCs without peptide loading, clearly indicated a HSP105 A2-7 peptide-specific response in the $CD4^-$ spleen cells (Fig. 1B). These $CD4^-$ spleen cells ($2x10^4$/well) showed 55±29.7 spot counts/well in response to the BM-DCs pulsed with the HSP105 A2-7 peptide, whereas they showed 23±31.1 spot counts/well in the presence of

Table I. HSP105-derived peptides conserved between human and mouse HSP105 predicted to bind to HLA-A2 or HLA-A24.

Peptides	Position	Subsequent residue listing	HLA-A2 binding score
HSP105 A2-4	120-128	MLLTKLKET	107
HSP105 A2-5	141-149	VISVPSFFT	55
HSP105 A2-6	155-163	SVLDAAQIV	37
HSP105 A2-7	169-177	RLMNDMTAV	591
HSP105 A2-9	202-210	DMGHSAFQV	21
HSP105 A2-10	222-230	VLGTAFDPFL	759
HSP105 A2-12	275-284	KLMSSNSTDL	276
HSP105 A2-13	276-284	LMSSNSTDL	26
HSP105 A2-14	300-309	KMNRSQFEEL	50
HSP105 A2-15	304-313	SQFEELCAEL	32
HSP105 A2-16	313-321	LLQKIEVPL	36
HSP105 A2-19	434-442	FLRRGPFEL	43
HSP105 A2-20	458-467	KIGRFVVQNT	76
HSP105 A2-25	668-676	LLTETEDWL	401
HSP105 A2-26	675-684	WLYEEGEDQA	146
HSP105 A2-29	757-765	EVMEWMNNV	15

Peptides	Position	Subsequent residue listing	HLA-A24 binding score
HSP105 A24-1	180-188	NYGIYKQDL	240
HSP105 A24-2	214-223	AFNKGKLKVL	30
HSP105 A24-3	251-260	KYKLDAKSKI	110
HSP105 A24-4	305-313	QFEELCAEL	47
HSP105 A24-5	433-442	TFLRRGPFEL	33
HSP105 A24-6	613-622	MYIETEGKMI	90
HSP105 A24-7	640-649	EYVYEFRDKL	330
HSP105 A24-8	725-733	HYAKIAADF	140
HSP105 A24-9	739-748	KYNHIDESEM	82

The binding scores were estimated by using BIMAS software: http//bimas.dcrt.nih.gov/cgi-bin/molbio/ken_parker_comboform.

BM-DCs pulsed with the HSP105 A2-4 peptide. A similarly strong response was observed for the HSP105 A24-7 peptide (Fig. 1C). $CD4^-$ spleen cells ($2x10^4$/well) showed 79.5±27.6 spot counts/well in response to the BM-DCs pulsed with the HSP105 A24-7 peptide, whereas they showed 20.5±14.8 spot counts/well in the presence of BM-DCs with the HSP A24-6 peptide. These assays were performed twice with similar results and they suggest that the HSP105 A2-7 and A24-7 peptides are potential CTL epitope peptides in both HLA Tgm and humans.

Identification of a CTL epitope in BALB/c mice and CTLs that are cytotoxic against C26 tumors in mice. There were similar structural motifs within the peptides that bound to human HLA-A24 and mice K^d. We selected those peptides with binding motifs for both HLA-A24 and K^d molecules and prepared 9 different synthetic peptides (HSP105-1-9). When we tested these peptides for their potential to induce *in vitro* tumor reactive CTLs in spleen cells derived from BALB/c mice immunized with the HSP105 peptides, only the HSP105 24-1 peptide-induced CTLs showed specific cytotoxicity against C26 tumors ($HSP105^+$, $H\text{-}2K^d$) (Fig. 2). The cytotoxicity against C26 was attenuated by HSP105 siRNA. These findings indicate that the HSP105 A24-1 peptide has the capacity to induce tumor reactive CTLs and that peptide vaccination-primed CTLs are reactive to this peptide *in vivo*. We would expect this HSP105 A24-1 (NYGIYKQDL) peptide to also be an epitope for human CTLs.

HSP105-reactive CTLs from PBMCs of HLA-A2-positive colorectal cancer patients and CTLs induce cytotoxicity against HSP105-expressing cancer cells. We generated a CTL line from PBMCs of colorectal patients by stimulation with the HSP105 A2-12 peptide. As shown by ^{51}Cr release assays, the resulting CTLs showed HSP105-specific cytotoxicity against SW620 cells ($HSP105^{+++}$, HLA-A2) and against T2 cells pulsed with the HSP105 A2-12 peptide ($HSP105^-$, HLA-A2), but not against HepG2 cells ($HSP105^{\pm}$, HLA-A2) or T2 cells pulsed with an irrelevant peptide (Fig. 3A). HSP105 siRNA decreased the cytotoxicity against SW620 cells. We investigated the effects of the HSP105 A2-12 peptide-reactive CTL lines on the mice implanted with the SW620 cells. Fourteen days after inoculation of HSP105 A2-12 peptide-reactive CTLs, there was an apparent reduction in tumor size in the SW620 compared to that in untreated mice (Fig. 3B). These results clearly indicate the efficacy of HSP105 A2-12 (KLMSSNSTDL) peptide-reactive CTL injection therapy for $HSP105^+$ tumors in mice.

Detection of HSP105-specific CTLs in peripheral blood of pre-surgical patients with colorectal cancer. Our results suggest that the four peptides, HSP105 A2-7 (RLMNDMTAV), HSP105 A2-12 (KLMSSNSTDL), HSP105 A24-1 (NYGIYK QDL) and HSP105 A24-7 (EYVYEFRDKL), are HSP105-derived, HLA-A2, or HLA-A24-restricted CTL epitopes. To determine the frequencies of the HSP105-derived T cells specific for these peptide in pre-surgical colorectal cancer patients, we analyzed the PBMC responses for each peptide using the ELISPOT assay. HSP105 expression was detected in 20 of 21 (95%) patients, consistent with previous studies (4). HSP105-specific T cells secreting IFN-γ were detected in patients stimulated with the HSP105 A2-7 (4 patients), HSP105 A2-12 (6 patients), HSP105 A24-1 (2 patients) and HSP105 A24-7 (6 patients) peptides (Table II). ELISPOT assay detected positive IFN-γ responses to at least one of the HSP105-derived peptides in PBMCs in 14 of the 21 patients. In contrast to the results for colorectal cancer patients, the 4 peptides were not recognized by PBMCs from healthy donors. Both the ratio of normal donors who showed positive T-cell responses to CMV-derived peptides and the frequencies of the specific T cells were identical to those of the colorectal cancer patients (data not shown).

HSP105-derived peptide immunization does not induce autoimmunity in HLA-A2 Tgm. HSP105 in normal adult mice is expressed in only certain tissues, and expression in these tissues is less than that in C26 tumor cells, suggesting a low

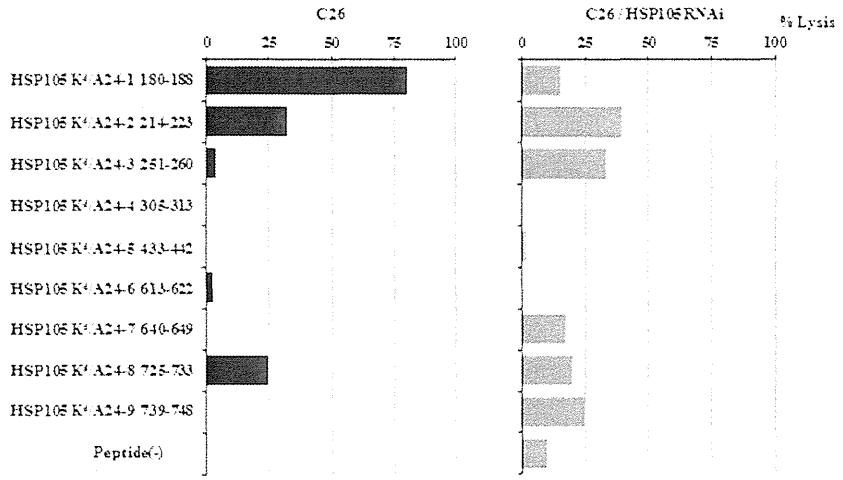

Figure 2. Identification of an HSP105-derived HLA-A24 and K^d-restricted CTL epitope. BALB/c mice were immunized with 9 HSP105 peptides. Using the ^{51}Cr release assay, sensitized spleen cells that had been stimulated *in vitro* with each HSP105 peptide (10 μmol/l) and cultured for 5 days with 100 U/ml interleukin-2 were examined for CTL activity against C26 cells and C26 cells transfected with HSP105 siRNA (C26/HSP105 RNAi). Values represent the percentage of specific cell lysis, based on the mean values from triplicate assays.

Table II. Expression of HSP105 in colorectal cancer tissue and quantification of HSP-specific CTLs in colorectal cancer patients.

						[c]Spot number of peptide-specific CTLs				
HLA-A2-positive patients	Age (yrs.)	Gender	HLA	Stage[a] of tumor	HSP105 expression[b]	HSP105 A2-7		HSP105 A2-12		CMV
1	62	M	0201/2601	IIIB	++	27	+	126	+	160
5	79	M	0207/1101	IIIB	++	0	-	2	-	10
6	51	M	0201/0206	I	+	0	-	49	+	136
8	55	M	0206/2402	I	±	0	-	0	-	66
11	69	M	0206/2402	IIIC	+	143	+	0	-	0
12	61	M	0201/3303	I	±	2	-	45	+	367
13	64	F	0201/2601	IIIC	±	0	-	2	-	254
14	66	M	0206/2402	IIIC	-	13	+	0	-	58
15	78	M	0201/1101	IIA	+	0	-	5	+	57
16	51	F	0206/2601	IV	±	31	+	7	+	15
17	63	F	0206/1101	IIA	++	0	-	25	+	96
HLA-A2402-positive patients						HSP105 A24-1		HSP105 A24-7		CMV
2	64	F	2402	IV	++	2	-	44	+	6
3	60	M	2402/3101	IIIC	++	0	-	0	-	11
4	71	F	2402/3101	IIA	++	25	+	51	+	12
7	47	M	2402/3101	IIIA	++	4	-	6	+	3
9	66	M	2402	IV	++	8	+	6	+	7
10	60	M	2402/3101	I	++	1	-	19	+	26
18	64	M	1101/2402	IV	+	0	-	2	-	40
20	46	F	1101/2402	IIIB	++	4	-	7	+	5
21	66	F	2402	I	++	3	-	0	-	38

F, female; M, male. [a]Stage, staging was performed according to the TNM classification (Union for International Cancer Control; UICC). [b]HSP105 expression, staining intensity of tumor cells was scored on a scale according to the following four grades: -, absent; ±, weak; +, moderate; ++, strong. [c]Spot number indicates the number of peptide-specific CTLs calculated by subtracting the spot number in a well of no peptide. -, Spot number <5; +, Spot number ≥5.